INTERNATIONAL JOURNAL FOR NUMERICAL METHODS IN FLUIDS, VOL. 19, 869–888 (1994)

PREDICTION OF TURBULENT WALL SHEAR FLOWS DIRECTLY FROM WALL

SHENQ-YUH JAW

Department of Naval Architecture, National Taiwan Ocean University, Keelung, Taiwan, R.O.C.

AND

ROBERT R. HWANG

Science and Engineering College, National Taiwan Ocean University, Keelung, Taiwan, R.O.C.

SUMMARY

The fully elliptic Reynolds-averaged Navier–Stokes equations have been used together with Lam and Bremhorst's low-Reynolds-number model, Chen and Patel's two-layer model and a two-point wall function method incorporated into the standard k–ε model to predict channel flows and a backward-facing step flow. These flows enable the evaluation of the performance of different near-wall treatments in flows involving streamwise and normal pressure gradients, flows with separation and flows with non-equilibrium turbulence characteristics. Direct numerical simulation (DNS) of a channel flow with $Re = 3200$ further provides the detailed budgets of each modelling term of the k and ε-transport equations. Comparison of model results with DNS data to evaluate the performance of each modelling term is also made in the present study. It is concluded that the low-Reynolds-number model has wider applicability and performs better than the two-layer model and wall function approaches. Comparison with DNS data further shows that large discrepancies exist between the DNS budgets and the modelled production and destruction terms of the ε equation. However, for simple channel flow the discrepancies are similar in magnitude but opposite in sign, so they are cancelled by each other. This may explain why, even when employing such an inaccurately modelled ε-equation, one can still predict satisfactorily some simple turbulent flows.

KEY WORDS k-ε model Two-layer model Low-Reynolds number model Wall function method

1. INTRODUCTION

The advancement of large computers has led to the wide use of higher-order turbulence models to predict turbulent flows. The most popular class includes the two-equation models in which two partial differential equations are used to describe the development of turbulent kinetic energy and of a quantity related to the turbulence length scale.[1–3] One such model is the k–ε eddy viscosity turbulence model, where k represents the turbulent kinetic energy, ε represents the dissipation rate of turbulent kinetic energy and the eddy viscosity is defined as $\upsilon_t = C_\mu k^2/\varepsilon$. Using the two quantitites k and ε, the turbulence length scale is self-determine from $k^{1.5}/\varepsilon$ and hence, unlike with some simpler models such as the mixing length model, the artificial introdution of a turbulence length scale is not necessary. This model has been successfully applied in many engineering applications of high-Reynolds-number turbulent flows. However, owing to the inexact modelling of the ε-transport equation, predictions of near-wall or low-Reynolds-number turbulent flows are still difficult and inaccurate unless special near-wall treatments are adopted.

CCC 0271–2091/94/220869–20

Received October 1993
Revised May 1994

When applying the k–ε model to solve wall turbulent flows, wall functions are usually adopted in the near-wall region. The so-called wall functions relate surface boundary conditions to points in the fluid away from the boundaries and thereby avoid the problem of modelling the direct influence of viscosity. The validity of this procedure is of course restricted to situations in which the Reynolds number is sufficiently high for the viscous effects to be unimportant or where universal wall functions are well established. There are a number of instances in which this approach has to be abandoned, e.g. turbulent boundary layers at low and transitional Reynolds numbers, unsteady and separated flows and the flow over spinning surfaces or surfaces with mass or heat transfer. Also, traditional wall functions are probably inappropriate for complex three-dimensional flows.

Predicting turbulent wall shear flows directly from the wall is attractive from a practical standpoint. Since the momentum and continuity equations are solved up to the wall, it provides the means to include the complexities of complex turbulent flows without invoking wall functions. Over the past years many suggestions have been made for the extension of turbulence closure models to enable their use at low Reynolds numbers and to describe the flow close to a solid wall. These suggestions can be divided into two main categories, namely the low-Reynolds-number model and the two-layer model. In a low-Reynolds-number turbulence model special damping functions are adopted to achieve the observed reduction of turbulent transport quantities very near the wall. Most low-Reynolds-number models are based on the same k–ε model and differ from one another in the damping functions. Reviews of various low-Reynolds-number models can be found in References 4–6. Employing a low-Reynolds-number model requires a fine grid system and small time steps, otherwise the numerical calculation may not converge. In general it requires more than 60 grid nodes within the boundary layer to get a converged solution from an initially guessed flow field. For a practical engineering application one would prefer a simpler model which is insensitive to the grid system and can be easily applied. The two-layer model was thus proposed. In a two-layer model the k–ε model is used only in the high-Reynolds-number regions and the viscosity-affected near-wall region is resolved with a simpler one-equation model involving a length scale prescription. The rate of energy dissipation and the eddy viscosity can then be expressed as algebraic relations of turbulent kinetic energy and the length scale prescription. Since the numerical difficulties encountered in low-Reynolds-number models are mainly introduced from the modelled ε-differential equation,[7] adopting an algebraic ε-equation will of course avoid such numerical instability problems. Different two-layer models differ from one another in the algebraic ε-equations or empirical coefficients. A review of two-layer models can be found in Reference 8.

In this study a general control volume[9] numerical method for the solution of the fully elliptic Reynolds-averaged Navier–Stokes equations is used in conjunction with a low-Reynolds-number model, a two-layer model and the wall function approach to evaluate the relative merits of various treatments of the near-wall flow. In particular, one of the more promising two-equation low-Reynolds-number models identified in Reference 4, namely that of Lam and Bremhorst,[10] the two-layer model of Chen and Patel,[11] which combines the standard k–ε model with the one-equation model of Wolfshtein[12] in the near-wall region, and the two-point wall function approach of Chen[13] are used to calculate unseparated channel flow and separated backward-facing step flow for which experimental data are available from References 14 and 15 respectively. Direct numerical simulation (DNS) of a low-Reynolds-number channel flow[16] further provides a complete database to develop and test models. Term-by-term comparisons with the DNS data are also made to investigate the performance of each modelling term of the k- and ε-transport equations.

2. GOVERNING EQUATIONS

Detailed derivations of the Reynolds-averaged Navier–Stokes equations and modelling of the k-ε turbulence transport equations can be found in Reference 7. Consequently, we outline here only the equations that are adopted for the study of near-wall turbulence models in the two-dimensional channel flows and backward-facing step flow.

Reynolds-averaged Navier–Stokes equations

The dimensionless Reynolds-averaged equations of continuity and momentum for steady, two-dimensional mean flow in Cartesian co-ordinates are

$$\frac{\partial U}{\partial X} + \frac{\partial V}{\partial Y} = 0, \tag{1}$$

$$U\frac{\partial U}{\partial x} + V\frac{\partial U}{\partial Y} = \frac{\partial}{\partial X}\left(\frac{1}{Re}\frac{\partial U}{\partial X}\right) + \frac{\partial}{\partial Y}\left(\frac{1}{Re}\frac{\partial U}{\partial Y}\right) - \frac{\partial}{\partial X}(\overline{u^2}) - \frac{\partial}{\partial Y}(\overline{uv}) - \frac{\partial P}{\partial X}, \tag{2}$$

$$U\frac{\partial V}{\partial X} + V\frac{\partial V}{\partial Y} = \frac{\partial}{\partial X}\left(\frac{1}{Re}\frac{\partial V}{\partial X}\right) + \frac{\partial}{\partial Y}\left(\frac{1}{Re}\frac{\partial V}{\partial Y}\right) - \frac{\partial}{\partial X}(\overline{uv}) - \frac{\partial}{\partial Y}(\overline{v^2}) - \frac{\partial P}{\partial Y}. \tag{3}$$

Here (U, V) are the mean velocity components and (u, v) are the fluctuating velocity components in the (X, Y)-directions respectively, P is the pressure and Re is the flow Reynolds number. The bar ($\overline{\ }$) over a quantity denotes the ensemble average.

Turbulence models

In the present study the eddy viscosity k–ε turbulence model is adopted, i.e. the Reynolds stresses are related to the corresponding mean rates of strain through the Boussinesq eddy viscosity model:

$$-\overline{u_i u_j} = \nu_t\left(\frac{\partial U_i}{\partial X_j} + \frac{\partial U_j}{\partial X_i}\right) - \tfrac{2}{3}\delta_{ij}k.$$

Here ν_t, the isotropic eddy viscosity, is related to the turbulence kinetic energy k, its rate of dissipation ε and a damping function f_μ by $\nu_t = C_\mu f_\mu k^2/\varepsilon$, C_μ is a constant, $C_\mu = 0{\cdot}09$. Hence for two-dimensional flow

$$-\overline{uu} = 2\nu_t\frac{\partial U}{\partial X} - \tfrac{2}{3}k,$$

$$-\overline{vv} = 2\nu_t\frac{\partial V}{\partial Y} - \tfrac{2}{3}k,$$

$$-\overline{uv} = \nu_t\left(\frac{\partial V}{\partial X} + \frac{\partial U}{\partial Y}\right).$$

The governing equation (1)–(3) then become

$$\frac{\partial U}{\partial X} + \frac{\partial V}{\partial Y} = 0, \tag{4}$$

$$U\frac{\partial U}{\partial X} + V\frac{\partial U}{\partial Y} = \frac{\partial}{\partial X}\left[\left(\frac{1}{Re} + \upsilon_t\right)\frac{\partial U}{\partial X}\right] + \frac{\partial}{\partial Y}\left[\left(\frac{1}{Re} + \upsilon_t\right)\frac{\partial U}{\partial Y}\right] + \frac{\partial}{\partial X}\left(\upsilon_t \frac{\partial U}{\partial X}\right) + \frac{\partial}{\partial Y}\left(\upsilon_t \frac{\partial V}{\partial X}\right) - \frac{2}{3}\frac{\partial k}{\partial X} - \frac{\partial P}{\partial X}, \tag{5}$$

$$U\frac{\partial V}{\partial X} + V\frac{\partial V}{\partial Y} = \frac{\partial}{\partial X}\left[\left(\frac{1}{Re} + \upsilon_t\right)\frac{\partial V}{\partial X}\right] + \frac{\partial}{\partial Y}\left[\left(\frac{1}{Re} + \upsilon_t\right)\frac{\partial V}{\partial Y}\right] + \frac{\partial}{\partial X}\left(\upsilon_t \frac{\partial U}{\partial Y}\right) + \frac{\partial}{\partial Y}\left(\upsilon_t \frac{\partial V}{\partial Y}\right) - \frac{2}{3}\frac{\partial k}{\partial Y} - \frac{\partial P}{\partial Y}. \tag{6}$$

These equations can be solved for (U, V, P) when the k–ε turbulence model is employed for the eddy viscosity distribution. Here k and ε are obtained from the transport equations

$$\frac{Dk}{Dt} = \frac{\partial}{\partial X}\left[\left(C_k f_\mu \frac{k^2}{\varepsilon} + \frac{1}{Re}\right)\frac{\partial k}{\partial X}\right] + \frac{\partial}{\partial Y}\left[\left(C_k f_\mu \frac{k^2}{\varepsilon} + \frac{1}{Re}\right)\frac{\partial k}{\partial Y}\right] - \mathscr{P} - \varepsilon. \tag{7}$$

$$\frac{D\varepsilon}{Dt} = \frac{\partial}{\partial X}\left[\left(C_\varepsilon f_\mu \frac{k^2}{\varepsilon} + \frac{1}{Re}\right)\frac{\partial \varepsilon}{\partial X}\right] + \frac{\partial}{\partial Y}\left[\left(C_\varepsilon f_\mu \frac{k^2}{\varepsilon} + \frac{1}{Re}\right)\frac{\partial \varepsilon}{\partial Y}\right] - \frac{\varepsilon}{k}(C_{\varepsilon 1} f_1 \mathscr{P} - C_{\varepsilon 2} f_2 \varepsilon), \tag{8}$$

where

$$\mathscr{P} = \upsilon_t\left[2\left(\frac{\partial U}{\partial X}\right)^2 + 2\left(\frac{\partial V}{\partial Y}\right)^2 + \left(\frac{\partial U}{\partial Y} + \frac{\partial V}{\partial X}\right)^2\right]$$

is the rate of production of k, $C_k = 0{\cdot}09$, $C_\varepsilon = 0{\cdot}07$, $C_{\varepsilon 1} = 1{\cdot}44$ and $C_{\varepsilon 2} = 1{\cdot}92$ are the turbulence model coefficients and f_μ, f_1 and f_2 are damping functions associated with low-Reynolds-number turbulence models. For the standard k–ε model these damping functions are set to be unity. Various near-wall treatments are discussed below.

In the wall function approach the first near-wall nodes are placed within the fully turbulent region. The transport equations (7) and (8) are solved, with $f_\mu = f_1 = f_2 = 1$, only in the region beyond some distance from the wall. The velocity components and corresponding turbulence parameters between the wall and the first near-wall nodes are usually obtained from separate analysis of the flow in the sublayer and buffer region using the logarithmic law of the wall and the associated equilibrium relations:

$$U_p^+ = U_p/U_\tau = (1/\kappa)\ln(EY_p^+), \tag{9}$$

$$k_p^+ = 1/(C_\mu)^{0.5}, \tag{10}$$

$$\varepsilon_p^+ = 1/\kappa Y_p^+, \tag{11}$$

$$\overline{uv}_p^+ = U_\tau^2 = 0{\cdot}3k_p^+, \qquad \text{for } 400 > Y_p^+ > 10,$$

or

$$U_p^+ = Y_p^+, \tag{12}$$

$$k_p^+ = 0{\cdot}1(Y_p^+)^2, \tag{13}$$

$$\varepsilon_p^+ = 0{\cdot}2, \tag{14}$$

$$\overline{uv}_p^+ = 0{\cdot}3k_p^+, \qquad \text{for } Y_p^+ < 10.$$

Here Y_p^+ is defined as $Y_p^+ = U_\tau Y_p/\upsilon$, Y_p is the dimensional normal distance from the wall, $U_\tau = (\tau_w/\rho)^{1/2}$ is the friction velocity, τ_w is the wall shear stress, $\kappa = 0{\cdot}418$ is the von Karman constant and $E = 9$. The two-point wall function approach[13] is adopted, i.e. two near-wall grid points are placed within the fully turbulent region which explicitly satisfy equation (9) or (12). An iterative solution of these equations then provides the value of U_τ and U_p, required to establish the boundary conditions, without any analysis of the flow in the sublayer and buffer region.

For low-Reynolds-number models damping functions have to be specified to approximate the observed reduction of turbulent quantities in the near-wall region. In the model of Lam and Bremhorst[10] they are

$$f_\mu = [1 - \exp(-0{\cdot}016R_y)]^2(1 + 19{\cdot}5/R_T), \tag{15}$$

$$f_1 = 1 + (0{\cdot}06/f_\mu)^3, \tag{16}$$

$$f_2 = 1 - \exp(-R_T^2), \tag{17}$$

where R_y and R_T are the turbulent Reynolds numbers

$$R_y = Rek^{1/2}Y, \qquad R_T = (k^2/\varepsilon)Re.$$

The constants in (15) and (16) are somewhat different from those quoted by Lam and Bremhorst,[10] the values used here being those recommended by Rodi.[17] Note that the damping functions considered above involve two turbulent Reynolds numbers R_y and R_T, which depend only on the local turbulence intensity k. In particular, the wall shear stress τ_w is not involved. Both R_y and R_T remain well defined in regions of flow reversal. Consequently, they can be applied in flows with separation.

In the two-layer approach the flow domain is divided into two regions. Region I includes the sublayer, the buffer layer and part of the fully turbulent layer. A one-equation model is employed in this region to count the wall proximity effects, whereas the standard k–ε model is used in region II. In the one-equation model only the turbulent kinetic energy is solved from a transport equation. The rate of energy dissipation in this region is specified by

$$\varepsilon = k^{3/2}/l_\varepsilon$$

and the eddy viscosity is obtained from

$$\upsilon_t = C_\mu k^{1/2} l_\mu,$$

where the length scales l_μ and l_ε contain the necessary damping effects in the near-wall region in terms of the turbulent Reynolds number R_y. For the one-equation model of Wolfshtein,[12] selected by Chen and Patel[11] in their two-layer model, l_μ and l_ε are specified as

$$l_\mu = C_l y[1 - \exp(-R_y/A_\mu)], \qquad l_\varepsilon = C_l y[1 - \exp(-R_y/A_\varepsilon)].$$

Note that both l_μ and l_ε become linear and approach $C_l y$ with increasing distance from the wall. Here C_l is given by

$$C_l = \kappa C_\mu^{-3/4}$$

to ensure a smooth eddy viscosity distribution at the junction of regions I and II. A_ε and A_μ are determined[11] somewhat differently from those reported in References 12 and 18. $A_\varepsilon = 2C_l$ is assigned so as to recover the proper asymptotic behaviour $\varepsilon = (2\nu k/y^2)$ in the sublayer and $A_\mu = 70$ is determined from a numerical test to match the logarithmic law in the case of a flat plate boundary layer. In region II, beyond the near-wall layer, the standard k–ε model is employed to calculate the velocity field as well as the eddy viscosity. The matching criterion between the one-equation and two-equation models is specified along a preselected grid line where the minimum R_y is of the order of 250, so that the damping effects are negligible. This ensures a smooth eddy viscosity distribution across the match boundary.

To solve the fully elliptic Reynolds-averaged Navier–Stokes equations (4)–(8), a computer code written by the finite volume method[9] with a staggered grid SIMPLER algorithm is used in the present study. The system of algebraic difference equations is solved by a line iteration method with alternating directions. The convergence criterion is specified as the relative difference of every dependent variable between time steps being smaller than 5×10^{-5}.

3. PREDICTION OF TWO-DIMENSIONAL CHANNEL FLOW

Consider a turbulent flow in a two-dimensional channel with dimensionless channel halfwidth and mean inlet velocity both equatl to unit. Computation is perfomed in the domain of width 1 × length 24. The channel halfwidth and mean inlet velocity are chosen as the length scale and velocity scale respectively. Based on these scales, the channel flow Reynolds number is 65,600, the same as that of Telbany and Reynolds' experiment.[14]

To avoid a large computational burden in calculating the flow development, the computation is started from the channel cross-section where the viscous layer thickness has developed to 85% of the channel halfwidth. In other words, the inlet condition is set at the cross-section where the viscous layer thickness $\delta = 0{\cdot}85$. The turbulent channel flow is considered as fully developed when the viscous layer has grown to be equal to the channel halfwidth of $\delta = 1$, which occurs at the locatin $X = 9$.[19] The computation domain is extended down to the location $X = 24$ and experimental data are given at $X = 22$.

Four boundary conditions for each governing equation (4)–(8) are required to make the problem well posed. The mean inlet velocity U_i is determined from the power law distribution

$$\frac{U_i}{U_{Ci}} = \left(\frac{1 - Y}{\delta}\right)^{1/7} = \left(\frac{1 - Y}{0{\cdot}85}\right)^{1/7} \quad \text{for } 1 - Y < 0{\cdot}85,$$

$$U_i = U_{Ci} = 1{\cdot}1 \quad \text{for } 1 - Y > 0{\cdot}85,$$

where U_{Ci} is the centreline inlet velocity. Note that the origin of the Y-co-ordinate is set at the centreline of the channel, while the boundary layer thickness is calculated from the wall

boundary, i.e. $Y = 1$. The inlet condition of turbulent kinetic energy, k_i, is determined from the experimental data of Telbany and Reynolds[14] measured in the fully developed region:

$$k_i = 0{\cdot}0099 - 0{\cdot}013Y + 0{\cdot}0057Y^2 + 0{\cdot}0001Y^3.$$

For the rate of kinetic energy dissipation, ε_i is taken to be

$$\varepsilon_i = k_i^{3/2}.$$

Note that ε cannot be measured by experiment. It is estimated from dimensional analysis by observing that the units of ε are equal to the units of k divided by a length scale. Several different initial conditions for k and ε were tested and it was found that the predicted results were insensitive to these conditions. Since the outlet section is in the fully developed region, the gradients of all variables U, V, k and ε in the flow direction, $\partial/\partial X$, are zero. On the centreline all variables satisfy the symmetric boundary condition $\partial/\partial Y = 0$. Along the wall differnt treatments have to be used for different models. In the wall function approach the flow characteristics between the first grid points and the wall are determined either from equation (9)–(11) or from equation (12)–(14), depending on their dimensionless normal distance to the wall. For the low-Reynolds-number model and the two-layer model the boundary conditions are specified on the wall; hence U, V and k are zero owing to the no-slip condition. For ε the wall condition is specified as $\partial\varepsilon/\partial Y = 0$ for the low-Reynolds-number model. The two-layer model does not need a wall condition for ε, since an algebraic equation is used in the near-wall layer.

A non-uniform grid system of 42×24 is used for the wall function method. Since the low-Reynolds-number model and the two-layer model require a finer grid system, 62×49 grid points are used for these two models. The computation is carried out with a time-marching scheme. Between time steps the dimensionless dependent variables are checked. If the relative difference of these variables, i.e. U, V, k and ε, at all nodal points are smaller than 5×10^{-5}, the solution is considered converged and the calculation is terminated. In the two-layer model calculation satisfactory convergence was obtained in less than 200 time steps. The low-Reynolds-number model was incorporated after the two-layer solution had converged in order to accelerate convergence and save computing time. Another 200 iterations with a smaller time step are required to meet the convergence criterion.

Figure 1 compares the predicted mean velocity profiles with the experimental data of Telbany and Reynolds[14] at three different locations. One is in the developing region, $X = 3{\cdot}5$, and the other two are in the fully developed region, $X = 13{\cdot}5$ and 22, as shown in Figures 1(a)–1(c) respectively. It is clear that all three approaches yield almost identical mean velocity profiles, presumably owing to the use of the same turbulence model for the flow outside the near-wall region. Figures 2(a)–(d) compare the predicted turbulent kinetic energy and Reynolds stress distributions with experimental data at the location $X = 22$. These calculated turbulence intensities are somewhat more sensitive to the near-wall treatments. The low-Reynolds-number model and the two-layer model yield identical profiles except in the near-wall region, while the wall function approach presents larger differences from the former two models. Note also that larger deviations exist between the calculate Reynods stresses and the experimental data, since the simple Boussinesq eddy viscosity approximation was adopted. To improve the Reynolds stress prediction, differential stress equations have to be employed.[7] Figure 3 shows the predicted production and dissipation of the turbulent kinetic energy budget. They are opposite in sign but about equal in magnitude, so the fully developed channel flow is in an equilibrium status.

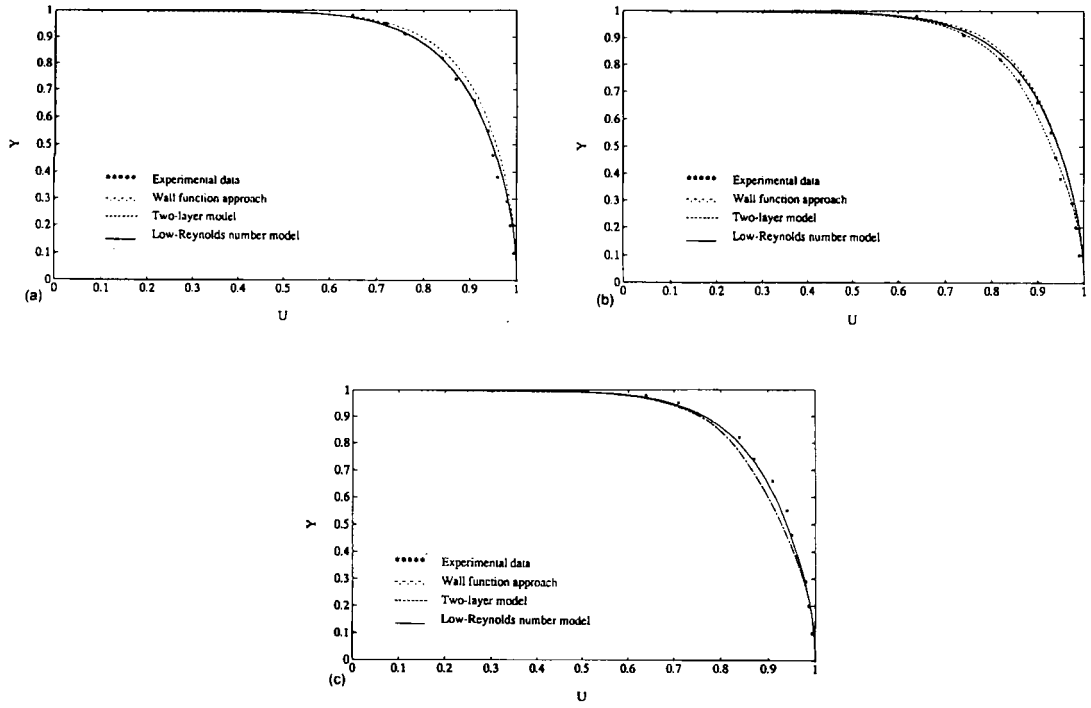

Figure 1. Velocity profiles of channel flows at (a) $X = 3{\cdot}5$, (b) $X = 13{\cdot}5$ and (c) $X = 22$

Since the wall function approach is derived under the assumption that the turbulent flow is parallel to the wall and in an equilibrium status,[13] predicting the mean flow of a non-separated, equilibrium turbulent flow by the wall function approach is adequate. This is confirmed in this study by observing that all the profiles, including those obtained from the wall function, fit fairly well with the experimental data.

As noted earlier, direct numerical simulations of turbulent flows provide a complete database to develop and test turbulence models. In order to investigate the performance of each modelling term of the k- and ε-transport equations, the low-Reynolds-number channel flow simulated by DNS[16] is also computed. The simulated flow fields are for a channel flow at a Reynolds number $Re_\tau = u_\tau \delta/\upsilon = 180$ based on the kinematic viscosity υ, wall shear velocity u_τ and channel halfwidth δ. This corresponds to a Reynolds number of 3200 based on the mean centreline velocity and channel halfwidth δ. A grid system of 62×49 is used for the low-Reynolds-number model and the two-layer model. The wall function approximation was not performed in this category, since the whole computational domain is in the wall-function-dominated region $u_\tau \delta/\upsilon = \delta^+ = 180 < 400$. Therefore no individual modelling distribution is available. A similar problem was encountered in presenting the distribution of the modelled ε-equation of the two-layer model. Since the whole computational domain is within the algebraic-ε-equation-dominated region $R_y < 250$, no differential ε-equation is adopted in the two-layer model and hence no individual distribution of the modelled ε-equation is available. Only distributions of the k-equation can be presented for the two-layer model.

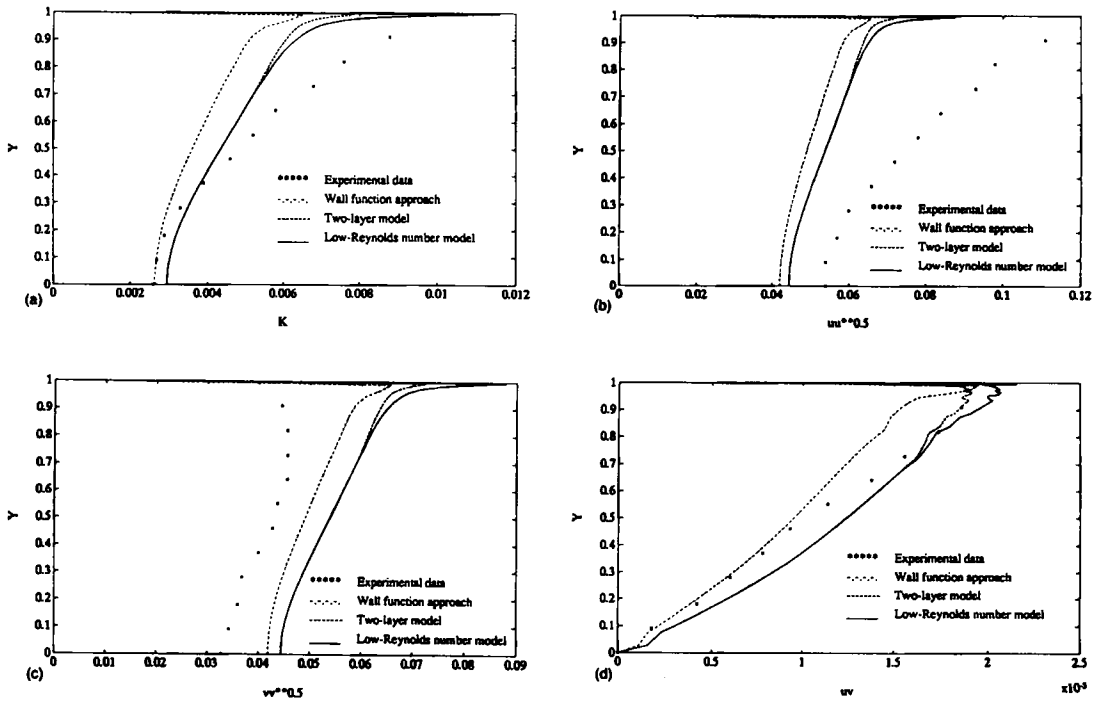

Figure 2. Turbulence characteristics of channel flow at $X = 22$: (a) turbulent kinetic energy; (b) Reynolds stress $(\overline{u^2})^{1/2}$; (c) Reynolds stress $(\overline{v^2})^{1/2}$; (d) Reynolds stress $\overline{uv}$

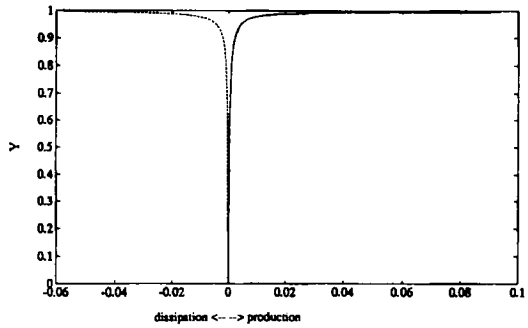

Figure 3. Production versus dissipation of turbulent kinetic energy

Similar boundary conditions to those stated above are used, except that the inlet velocity profile is modified in accordance with this Reynolds number as

$$\frac{U_i}{U_{Ci}} = \left(\frac{1-Y}{\delta}\right)^{1/6\cdot29} = \left(\frac{1-Y}{0\cdot85}\right)^{1/6\cdot29} \quad \text{for } 1-Y < 0\cdot85,$$

$$U_i = U_{Ci} = 1 \quad \text{for } 1-Y > 0\cdot85.$$

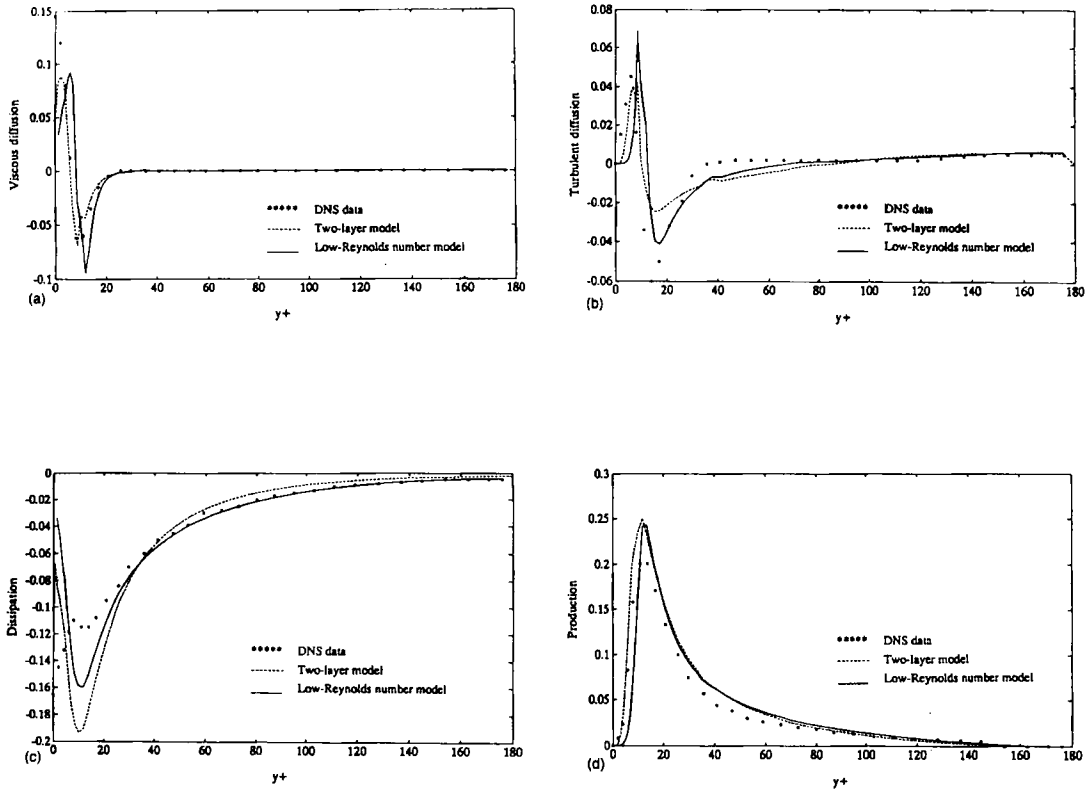

Figure 4. Budgets of k-transport equation: (a) Viscous diffusion; (b) turbulent diffusion; (c) dissipation; (d) production

The inlet condition for k and ε are assumed to be the same as those of high-Reynolds-number channel flow. Different inlet conditions were also tested and it was confirmed again that for equilibrium turbulent flows the predicted results were insensitive to the k, ε inlet conditions.[7]

Figure 4 compares the DNS budgets of exact turbulent kinetic energy with modelled k-budgets. Figures 4(a) and 4(b) show that for viscous diffusion,

$$\frac{\partial}{\partial X_l}\left(\upsilon \frac{\partial k}{\partial X_l}\right),$$

turbulent diffusion,

$$\frac{\partial}{\partial X_l}\left(-\overline{u_l k'} - \frac{\overline{pu_l}}{\rho}\right) = \frac{\partial}{\partial X_l}\left(C_k f_\mu \frac{k^2}{\varepsilon}\frac{\partial k}{\partial X_l}\right),$$

both models yield similar result to the DNS data, but the low-Reynolds-number model predicts larger diffusion effects and is closer to the DNS data. Figure 4(c) shows the dissipation budget of k. It is found that the two-layer model overpredicts its peak value, $\varepsilon(\text{peak}) = -0{\cdot}195$, while the low-Reynolds-number model predicts $\varepsilon(\text{peak}) = -0{\cdot}16$, closer to the DNS data, $\varepsilon(\text{peak}) = -0{\cdot}162$. Both profiles shift their peak position from the wall to about $Y^+ = 16$, the location of the second peak of the DNS data. It is interesting to point out that the dissipation budget deduced from experimental data of a flat plate boundary layer[4] also presents such a shift, but with a peak of 0·2, which is much closer to the two-layer profile. This is anticipated, since the model coefficients of the two-layer model were adjusted to fit the experimental data of a flat plate boundary layer. Figure 4(d) shows that for the production term

$$-\overline{u_i u_l}\frac{\partial U_i}{\partial X_l}$$

both the low-Reynolds-number model and the two-layer model overpredict their peak values, with $P(\text{peak}) = 0{\cdot}24$ for the low-Reynolds-number model and $P(\text{peak}) = 0{\cdot}25$ for the two-layer model. The DNS peak value is about $P(\text{peak}) = 0{\cdot}2$.

It should be pointed out that in the k-equation only the turbulent diffusion term requires a model. From Figure 4(b) it is known that the modelled diffusion term fits quite well with the DNS data. Hence the k-equation is considered to be relatively accurate, so that the prediction of k directly from the wall can be achieved without any modification.

Figure 5 compares the budgets of the modelled ε-equation with DNS data. As mentioned above, no ε-budgets of the two-layer model are available, so only budgets of the low-Reynolds-number model are compared. Figures 5(a) and 5(b) present the distributions of viscous diffusion,

$$\frac{\partial}{\partial X_l}\left(\upsilon\frac{\partial \varepsilon}{\partial X_l}\right),$$

and turbulent diffusion,

$$\frac{\partial}{\partial X_l}\left(C_\varepsilon f_\mu \frac{k^2 \partial \varepsilon}{\varepsilon \partial X_l}\right),$$

of ε versus DNS data. It is clear that for $Y^+ > 18$ the modelled diffusion terms match correctly with DNS data. For $Y^+ < 18$ an obvious disagreement exists in the turbulent diffusion term, especially in the region close to the wall, $Y^+ < 10$. However, the disagreement is small compared with the errors in other terms, since the magnitude of diffusion is about an order smaller than other modelling terms, as shown in the following figures. Figure 5(c) shows that the modelled destruction of ε,

$$-2\left(\upsilon\frac{\overline{\partial^2 u_i}}{\partial X_j \partial X_l}\right)^2 = -C_{\varepsilon 2} f_2 \frac{\varepsilon^2}{k},$$

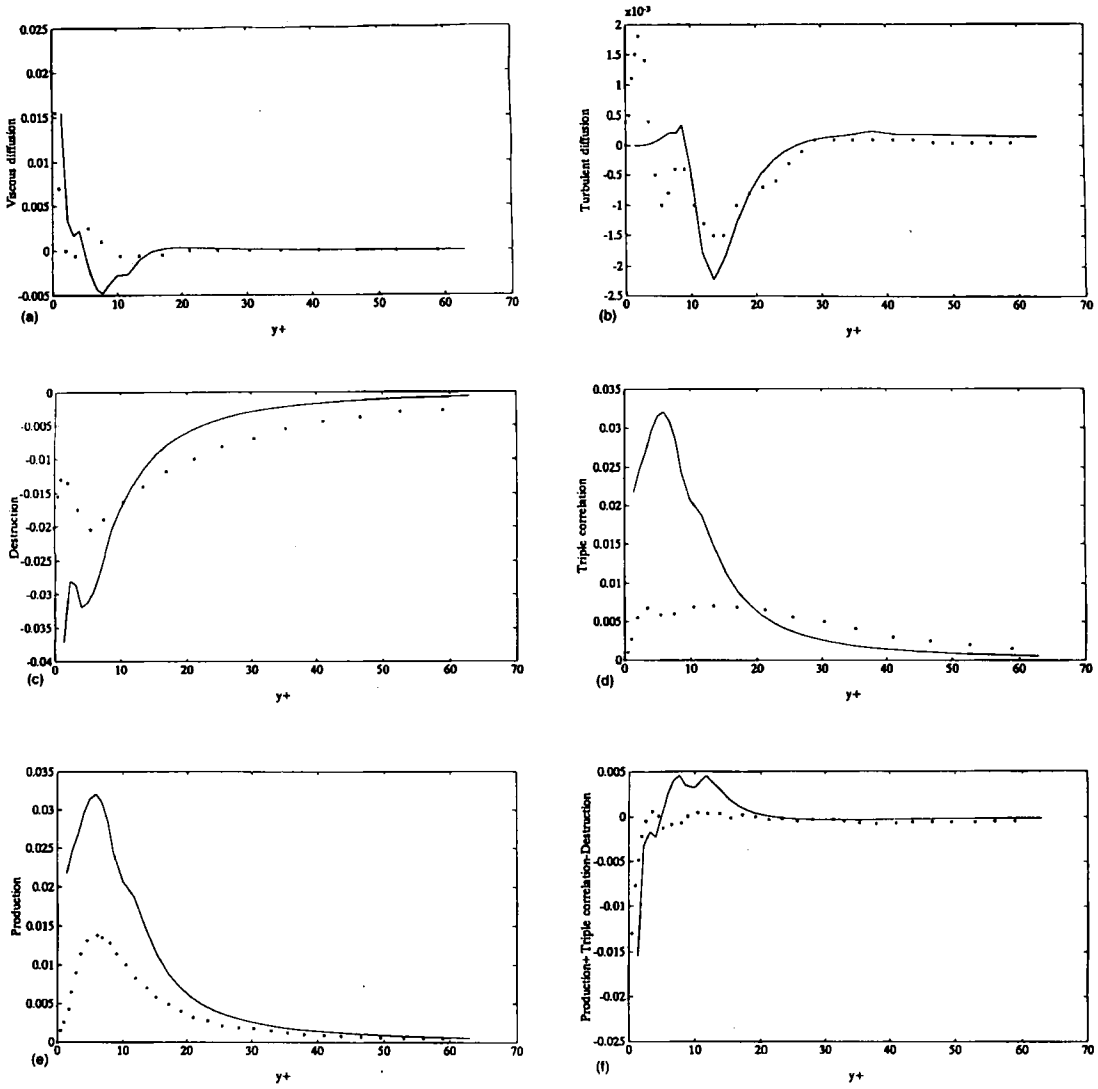

Figure 5. Budgets of ε-transport equation: (a) viscous diffusion; (b) turbulent diffusion; (c) destruction; (d) production versus triple correlation; (e) production versus exact production; (f) sum of production and destruction versus sum of exact production, triple correlation and destruction (see text for expressions)

is overpredicted even though the trend of the profile is correct. Figures 5(d) and 5(e) plot the modelled production term

$$-C_{\varepsilon 1} f_1 \frac{\varepsilon}{k} \overline{u_i u_l} \frac{\partial U_i}{\partial X_l}$$

with respect to the triple-correlation term

$$-2\upsilon \frac{\overline{\partial u_i \partial u_i \partial u_j}}{\partial X_j \partial X_l \partial X_l}$$

and the exact production term

$$-2\upsilon \frac{\partial U_i}{\partial X_j}\left(\frac{\overline{\partial u_i \partial u_j}}{\partial X_l \partial X_l} + \frac{\overline{\partial u_l \partial u_l}}{\partial X_i \partial X_j}\right)$$

respectively to see whether the modelled production comes from either of these two terms. From these two figures it is known that the modelled production fits neither of these two terms. However, if we plot the summation of modelled production and destruction with respect to the summation of exact production, triple-correlation and destruction terms, the curve fits much better with DNS data, as shown in Figure 5(f). The summation of errors is an order of magnitude smaller than the error in each individual term. This may explain why, even when using such an inaccurately modelled ε-equation, one can still predict correctly some simple turbulent flows. Since the modelled production and destruction terms yield errors with similar magnitude but opposite in sign, their errors are cancelled by each other. This may not be true, however, for more complex flows. In that case, using the k–ε model may cause greater error in predicting turbulent flows.

4. PREDICTION OF BACKWARD-FACING STEP FLOW

In this section we consider a turbulent flow past a backward-facing step. This flow has been extensively measured, since it is considered by many researchers and engineers as a fundamental configuration of internal flows. It provides turbulence models with additional test domain, since the flow separates at the step and reattaches downstream. The flow then recirculates behind the step. Prediction of this flow can thus enable one to examine the model capability in predicting not only the distribution of turbulence transport quantities but also the mean velocity distributions. The wall function proposed in equation (9)–(14) is known not to be appropriate for use near the points of separation and reattachment, since its basic assumptions conflict with the flow characteristics in those regions. The use of the wall function in predicting backward-facing step flow is mainly due to engineering simplification. Low-Reynolds-number models and two-layer models are applied directly up to the wall without adopting any approximation and hence are anticipated to perform better. The following is an attempt to examine the validity of the low-Reynolds-number model, the two-layer model and the wall function approach in predicting flow separation as it passes the backward-facing step.

Consider a two-dimensional channel flow past a step as shown in Figure 6. The dimensionless downstream channel half-height is $W = 1$, the upstream half-height is $H = \frac{2}{3}$ and the step height is $\frac{1}{3}$. W is chosen as the reference length scale, while the reference velocity scale is the mean inlet

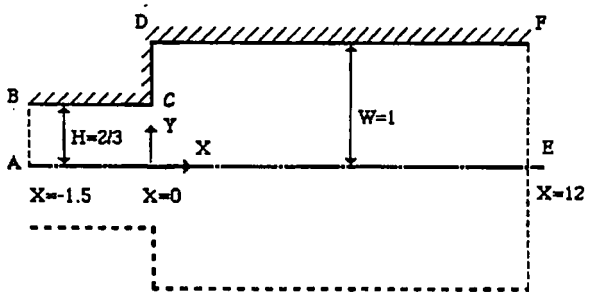

Figure 6. Computational domain of backward-facing step flow

velocity U_m. Based on these scales, the Reynolds number is 30,210 and the expansion ratio, defined as W/H, is 1·5, equivalent to the experimental set-up of Smyth.[15] It is known from experiments of Abott and Kline[20] that if the expansion ratio is equal to or less than 1·5, the turbulent flow is steady and the separation is symmetric in a symmetrical backward-facing step. Since the expansion ratio of the selected experiment is equal to 1·5, the flow pattern, according to Smyth,[15] is symmetric to the centreline. Therefore only the upper half of the channel with the backward-facing step is considered in this numerical calculation. As shown in Figure 6, the distance between the inlet and the step is taken to be 1·5 and the outlet is 12 units downstream from the step. Cartesian co-ordinates are used with the X-axis directed along the centreline and the origin at the step.

For the elliptic-type partial differential equations (4)–(8) to be well posed, suitably boundary conditions should be specified. Referring to Figure 6, these are specified as follows.

(1) *For the inlet A–B.* The inlet profiles of U, k and ε are specified at $X = -1{\cdot}5$ such that the predicted results fit Smyth's experimental data of U and $(\overline{u^2})^{1/2}$ at $X = 0$. Several inlet profiles were examined. The following profiles are selected for all the calculations:

$$U_i = 1{\cdot}17(1 - Y)^{1/7},$$

$$k_i = 0{\cdot}023 + 0{\cdot}19Y - 0{\cdot}799Y^2 + 1{\cdot}335Y^3,$$

$$\varepsilon_i = k_i^{3/2}.$$

A one-seventh power law velocity distribution is used as the inlet velocity boundary condition. A coefficient of 1·17 is multiplied in the velocity distribution since the maximum velocity is 1·17 times larger than the mean duct entry velocity. The k-profile was not provided by the experiment. It is determined empirically so that the predicted U- and $(\overline{u^2})^{1/2}$-profiles at the step entrance match closely with the experimental data. Finally, ε is estimated from dimensional analysis again.

(2) *For the outlet E–F.* Since the outlet E–F is sufficiently far downstream of the step, it is assumed that the flow is fully developed at the outlet. Thus the fully developed boundary condition $\partial/\partial X = 0$ is used for the variable U, V, k *and* ε.

(3) *For the solid walls B–C, C–D and D–E.* Similar wall conditions to those state in Section 3 are adopted. However, when applying the low-Reynolds-number model and the two-layer model in the step corner region, i.e. the junction between walls CD and DF, two different length scales were tested. One considers the damping effect induced by the nearest wall only, i.e. chooses the minimum distance measured from the two walls. The other then chooses the mean length scale, i.e. the root mean square of distances to both walls, $dl = [(dX)^2 + (dY)^2]^{0{\cdot}5}$, with dX and dY being the normal distances measured to walls CD and DF respectively. Comparing the computational results, it is found that most of the flow fields are similar, except in the corner region, where there is a second separation bubble present when using the minimum length scale in the low-Reynolds-number model. For the two-layer model the second separation bubble is present for both length scales, but with the shorter length scale adopted, a larger second separation bubble is predicted. It seems that using the shorter length scale can give a more detailed flow structure and hence it is adopted in the present study.

(4) Along the symmetric centreline A–F. The symmetric boundary condition $\partial/\partial Y = 0$ is used for all the variables.

Grid systems of 63 × 32 for the wall function approach and 68 × 36 for the low-Reynolds-number model and the two-layer model are used in the numerical calculations. Dense grids are placed near the solid wall where the velocity gradient is steeper and near the step where the

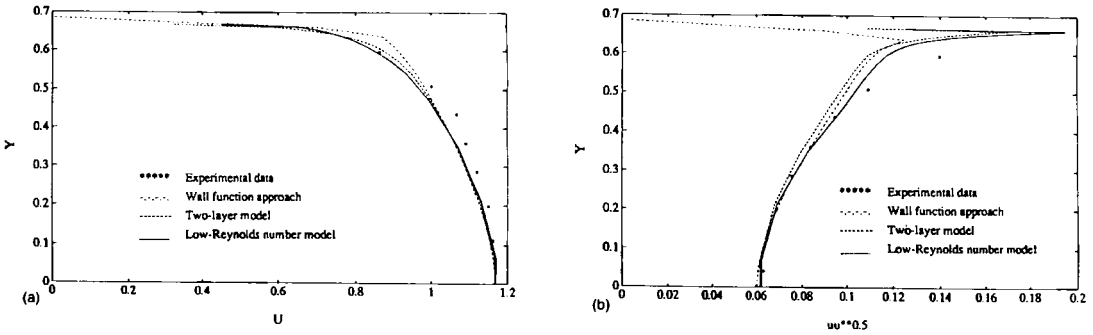

Figure 7. Profiles at step entrance: (a) U-velocity; (b) Reynold stress $(\overline{u^2})^{1/2}$

flow is expected to separate. The computation is also carried out with a time-marching scheme. The convergence criterion is set the same as in the channel flows.

Predicted results are compared with Smyth's[15] experiments. The profiles at the step expansion section are checked first. Since the flow is relatively sensitive to the upstream k, ε boundary conditions, adjustment of these two boundary conditions so that the predicted profiles match with the experimental data at the step expansion, $X = 0$, is necessary. Otherwise comparison of the profiles at downstream sections with experimental data would be meaningless. Figure 7 shows that all three turbulence models predict fairly close U- and $(\overline{u^2})^{1/2}$-profiles at the step entrance, $X = 0$, and thus comparison at downstream sections is meaningful.

Figure 8 shows the streamfunction contours predicted from the low-Reynolds-number model. This plot gives the upper half of the turbulent flow past a symmetrical backward-facting step. The rectangular block in the upper left corner of the figure is the channel step. Note that right on the step corner there is a tiny secondary separation bubble. A similar phenomenon was also observed by Rodi.[21] Checking the computational results, it is found that the predicted reattachment length extends to about $X = 1{\cdot}6$, $2{\cdot}4$ and $1{\cdot}0$ for the low-Reynolds-number model, the two-layer model and the wall function approach respectively, while the experimental data claim that $X = 1{\cdot}5$. The predicted reattachment length of the low-Reynolds-number model is much closer to the experimental data.

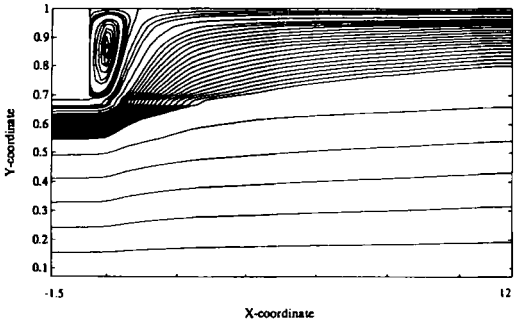

Figure 8. Streamfunction contours of low-Reynolds-number model

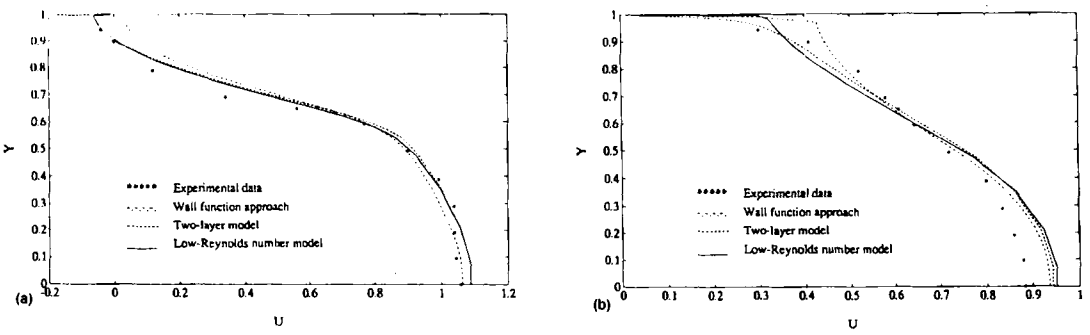

Figure 9. U-velocity profiles of backward-facing step flow at (a) $X = 1{\cdot}2$ and (b) $X = 4$

Figures 9–13 present comparisons of the mean velocity U, the turbulent kinetic energy k and the Reynolds stresses $(\overline{u^2})^{1/2}$, $(\overline{v^2})^{1/2}$ and $\overline{uv}$ respectively at two different cross-sections. One is within the recirculation zone, $X = 1{\cdot}2$, and the other is downstream of the recirculation zone, $X = 4$. For the velocity profiles, as shown in Figure 9, all three turbulence models predict similar results in the centreline region. Close to the wall the velocity profiles predicted by different near-wall treatments vary significantly, especially within the recirculation zone. In Figure 9(a) the near-wall velocities predicted by the low-Reynolds-number model and the two-layer model are negative, while those predicted by the wall function approach have become positive. The experimental data show that this section is still within the recirculatin zone; the near-wall velocity is negative and is consistent with the results of the low-Reynolds-number model and the two-layer model. However, the two-layer model overpredicts the reverse flow velocity and the reattachment length. The two-layer model seems to be sensitive to the adverse pressure gradients of separated flows. Remember that both the low-Reynolds-number model and the two-layer model predict almost identical profiles for a non-separated channel flow, but only the former predicts satisfactory the separated flow. In general the low-Reynods-number model predicts much better results than the two-layer model and the wall function approach.

Turbulent kinetic energy and Reynolds stress profiles are presented in Figures 10–13. From these figures it is known that the wall function approach predicts larger turbulence insensities and Reynolds stresses in the separation region. These stronger turbulence quantities will generate a stronger eddy viscosity and hence hamper the development of the separation region. Thus the

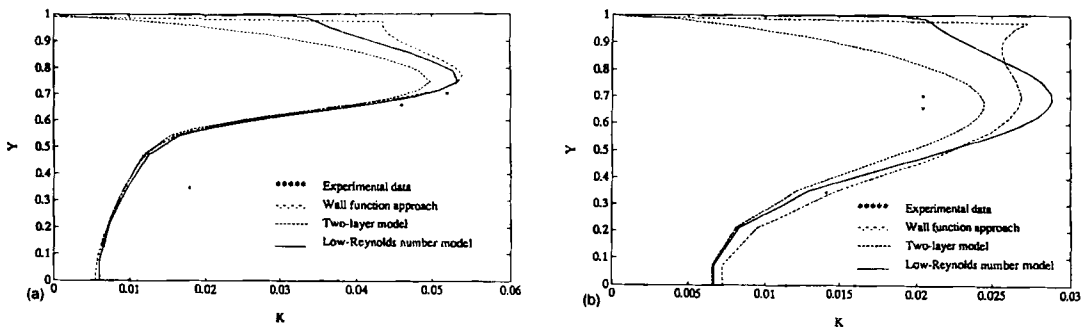

Figure 10. Turbulent kinetic energy profiles of backward-facing step flow at (a) $X = 1{\cdot}2$ and (b) $X = 4$

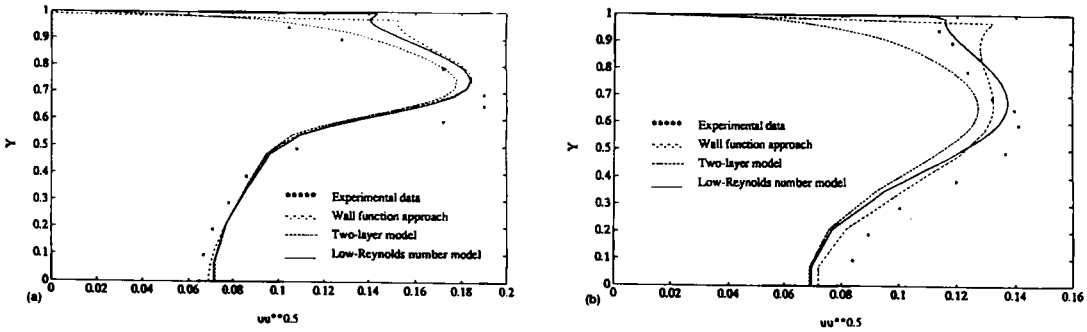

Figure 11. Reynolds stress $(\overline{u^2})^{1/2}$ at (a) $X = 1{\cdot}2$ and (b) $X = 4$

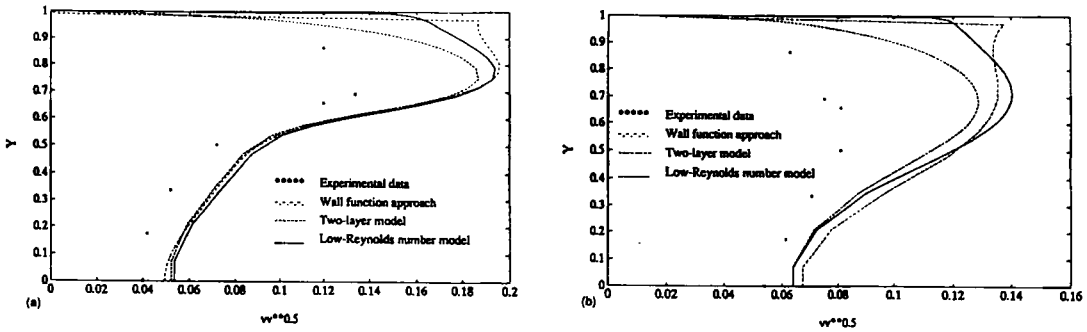

Figure 12. Reynolds stress $(\overline{v^2})^{1/2}$ at (a) $X = 1{\cdot}2$ and (b) $X = 4$

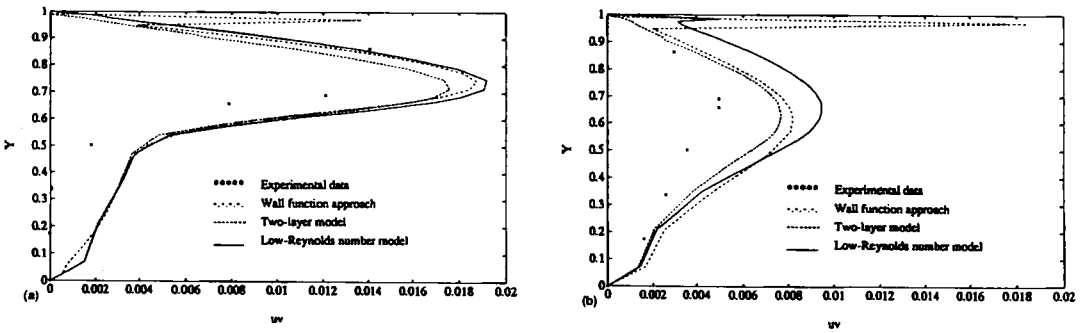

Figure 13. Reynolds stress $\overline{uv}$ at (a) $X = 1{\cdot}2$ and (b) $X = 4$

recirculation length predicted by the wall function approach is too short. In contrast, the two-layer model generally predicts smaller turbulence quantities, so its predicted recirculation length is too long.

Larger deviations are usually found in Reynolds stress distributions, especially the $(\overline{v^2})^{1/2}$- and $\overline{uv}$-profiles, since the simple Boussinesq eddy viscosity model was adopted. Predicted $(\overline{u^2})^{1/2}$-profiles are much closer to experimental data, since the inlet conditions are chosen so that the predicted $(\overline{u^2})^{1/2}$ match correctly with experimental data at the step entrance.

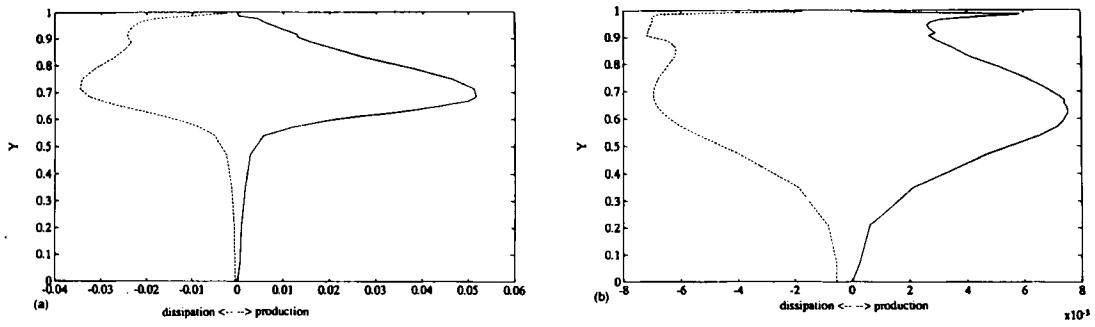

Figure 14. Production versus dissipation at (a) $X = 1{\cdot}2$ and (b) $X = 4$

The production and dissipation budgets of turbulent kinetic energy are plotted in Figure 14. It is found that within the recirculation zone, as shown in Figure 14(a), the production outweighs the dissipation, so the turbulent flow is not in equilibrium. Downstream of the recirculation zone, Figure 14(b), the production and dissipation tend to be equal and the turbulent flow is close to equilibrium. These results are helpful in explaining the inadequacy of applying wall functions in separation flow calculation. Since separation flow is neither parallel to the wall nor in an equilibrium status, employing the wall function approach in this region will of course introduce errors. In addition, the non-equilibrium status also induces the flow to be sensitive to the inlet boundary conditions.[7] Hence checking of the entrance profiles is necessary when solving such flows.

5. CONCLUDING REMARKS

The finite volume numerical method for the solution of the fully elliptic Reynolds-averaged Navier–Stokes equations have been used in conjunction with Lam and Bremhorst's low-Reynolds-number model, Chen and Patel's two-layer model and the two-point wall function method to evaluate the relative merits of various near-wall treatments in predicting wall turbulent flows. The selected test flows are the two-dimensional channel flows and the separated backward-facing step flow. These flows enable the evaluation of the performance of various near-wall treatments in flows with normal and streamwise pressure gradients, flow with separation and flow with non-equilibrium turbulence characteristics. Since complex turbulent flows usually bear such characteristics, predicting these flows will help in determining which model is more adequate to be employed in predicting complex turbulent flows. The results indicate that the wall function approach is too simplified and is inadequate in predicting complex flows. Models that can solve turbulent flows all the way to the wall, such as the low-Reynolds-number model and the two-layer model, are preferred. From the computation results it is found that only the low-Reynolds-number model predicts satisfactory all the flows considered. In general the low-Reynolds-number model has wider applicability and predicts better results than the wall function approach and the two-layer model. Nevertheless, when employing such a model, one may encounter various numerical difficulties such as grid sensitivity, slow convergence, etc. The present numerical scheme did not experience any special difficulty with the low-Reynolds-number model, since the latter was incorporated after the two-layer solution had converged. However, the computation did break down if the model was employed from the

beginning of the solution procedure. The numerical instability problems were not investigated in enough detail to give a rigorous explanation, since that was not the purpose of the present study.

For practical engineering applications a simpler model which has few numerical instability problems and is insensitive to the grid system is preferred. The idea of the two-layer approach was thus proposed. The two-layer approach is quite insensitive to the grid spacing and the number of grid points in the inner layer and to the location of the match boundary between the one- and two-equation models of the inner and outer layers. Its relative simplicity is attractive, because additional modifications and generalizations for more complex flows can be easily made. However, this model seems to be sensitive to the adverse pressure gradients of separated flows. Its performance in predicting backward-facing step flow is not as good as that of the low-Reynolds-number model.

Direct numerical simulation of a low-Reynolds-number channel flow provides the detailed budgets of each modelling term of the turbulent transport equations. Comparing the model results with DNS data can clearly manifest the performance of each modelling term of the turbulent transport equations. It is found that the modelled k-equation, which requires only one modelling term for the turbulent diffusion, fits quite well with DNS data and is considered to be relatively accurate. The modelled ε-equation, especially its production and destruction terms, deviates from DNS data significantly. Fortunately, the deviations of these two terms are similar in magnitude but opposite in sign. They are therefore cancelled by each other. This explains why, even when employing such an inaccurately modelled ε-equation, one can still predict satisfactorily some simple turbulent flows.

ACKNOWLEDGEMENT

This research was supported by the National Science Council, Taiwan, R.O.C. under contract NSC-81-0415-E-019-511.

REFERENCES

1. W. P. Jones and B. E. Launder, 'The prediction of laminarization with a two-equation model of turbulence', *Int. J. Heat Mass Transfer*, **15**, 301–314 (1972).
2. P. G. Saffman and D. C. Wilcox, 'Turbulent model predictions for turbulent boundary layers', *AIAA J.*, **12**, 541–546 (1974).
3. H. Vollmers and J. C. Rotta, 'Similar solutions of the mean velocity, turbulent energy and length scale equation.' *AIAA J.*, **15**, 714–720 (1977).
4. V. C. Patel, W. Rodi and G. Scheuerer, 'Turbulence models for near-wall and low Reynolds number flows: a review', *AIAA J.*, **23**, 1308–1319 (1984).
5. V. Michelassi and T.-H. Shih, 'Low Reynolds number two-equation modeling of turbulent flows.' *NASA Tech. Memo. 104368*, 1991.
6. R. M. C. So, Y. G. Lai and H. S. Zhang, 'Second-order near-wall turbulence closures: a review', *AIA J.*, **29**, 1819–1835 (1991).
7. S. Y. Jaw, 'Development of an anisotropic turbulence model for prediction of complex flows', *Ph.D. Dissertation*, University of Iowa, Iowa City, IA, 1991.
8. Y. C. Chang, 'Comparison study of two-layer turbulence models,' *Master Thesis*, National Taiwan Ocean University, Keelung, 1993 (in Chinese).
9. S. V. Patankar, *Numerical Heat Transfer and Fluid Flow*, Hemisphere, Washington, DC, 1972.
10. C. K. G. Lam and K. Bremhorst, 'A modified form of the k–ε model for predicting wall turbulence', *Trans. ASME*, **103**, 456–460 (1981).
11. H. C. Chen and V. C Patel, 'Near-wall turbulence models for complex flows including separation', *AIAA J.*, **26**, 641–648 (1988).
12. M. Wolfshtein, 'The velocity and temperature distribution in one-dimensional flow with turbulence augmentation and pressure gradient', *Int. J. Heat Mass Transfer*, **12**, 301–318 (1969).

13. C. J. Chen, 'Prediction of turbulent flows', Tech.Rep. 17, Central Research Institute of Electric Power Industry, Abiko, 1983.
14. M. M. M. Telbany and A. J. Reynolds, 'Turbulence in plane channel flows'. *J. Fluid Mech.*, **111**, 283–318 (1981).
15. R. Smyth, 'Turbulence flow over a plane symmetric sudden expansion', *J. Fluids Eng.*, **101**, 348–353 (1979).
16. N. N. Mansour, J. Kim and P. Moin, 'Reynolds-stress and dissipation rate budgets in a turbulent channel flow', *J. Fluid Mech.*, **194**, 15–44 (1988).
17. W. Rodi, 'Examples of turbulence models for imcompressible flows', *AIAA J.*, **20**, 872–879 (1982).
18. B. E. Launder, 'Low-Reynolds-number turbulence near walls.' Rep. TFD/86/4, University of Manchester Institute of Science and Technology, Thermo-Fluids Division, 1986.
19. H. Schlichting, *Boundary-Layer Theory*, McGraw-Hill, New York, 1955.
20. D. E. Abott and S. J. Kline, 'Experimental investigation of subsonic flow over single and double backward facing steps'. *J. Basic Eng.*, **84**, 317–325 (1962).
21. W. Rodi 'Experience with two-layer models combining the k–ε model with a one-equation model near wall'. *Proc. 29th Aerospace Science Meet.*, Reno, NV, 1991.